**Proceedings of the ASME 2016 International Mechanical Engineering Congress and Exposition**
**IMECE2016**
**November 11-17, 2016, Phoenix, Arizona, USA**

# IMECE2016-65644

# ANALYSIS OF CURVED COMPOSITE STRUCTURES THROUGH REFINED 1D FINITE ELEMENTS WITH AEROSPACE APPLICATIONS

**Erasmo Carrera**
Department of Mechanical and Aerospace Engineering
Politecnico di Torino,
Torino, Piemonte, 10129
Italy
Email: erasmo.carrera@polito.it

**Alberto García de Miguel***
**Alfonso Pagani**
**Marco Petrolo**
Department of Mechanical and Aerospace Engineering
Politecnico di Torino,
Torino, Piemonte, 10129
Italy
Email: alberto.garcia@polito.it

## ABSTRACT

*This paper presents a novel approach to deal with the analysis of composite aerospace structures with curved sections. The Carrera Unified Formulation is exploited to create hierarchical high-order beam models capable of detecting both local and global mechanical behaviors of composite structures. The blending function method is applied to introduce the exact shape of the cross-section boundaries into the mapping functions. Problems at both microstructure scale (fiber-matrix system) and macrostructure scale (whole components) can be studied with no lack of generalization. Several numerical examples of aerospace structures are included and the results are compared against those from the literature, as well as solid solutions obtained through the commercial software MSC Nastran. From this study, it is clear than the present formulation has demonstrated to be a powerful tool for the study of composite structures, enabling to obtain complex 3D-like solutions with a substantial reduction in the computational costs.*

## INTRODUCTION

During the last decades, the use of composite materials has acquired a main role in the construction of new advanced structures. Major aerospace companies include these materials not only in secondary components but also in primary structures such as wings or fuselages. The advantages of composites are many, amongst them: high stiffness to weight ratio, high strength to weight ratio, fatigue strength, or ease of formability (see Tsai [1]). The development of accurate models for composite structures have become of main interest for the industry since it serves to get a better understanding of the behaviour of these materials in many environments. In this context, one-dimensional models represent an effective alternative to solid formulations, in particular when slender structures are considered. The classical beam theories, developed by Euler [2] and then by Timoshenko [3], do not always serve for the analysis of composites since they are not able to predict correctly shear effects, making it necessary to enhance one-dimensional models by using refined formulations. A well-known review of the first developments on laminated beams and plate models was written by Kapania and Raciti [4, 5]. The structural analysis of composite structures can be directed following two different approaches depending on the correlation between the number of layers and the number of degrees of freedom of the model: the Equivalent Single Layer and the Layer Wise. In the Equivalent Single Layer (ESL) approach, the number of degrees of freedom is independent of the number of components of the composite. Reddy [6] developed an ESL higher-order shear deformation theory for plates, which was then extended by Khedeir and Reddy [7, 8] for the analysis of free-vibrations and buckling of cross-ply beams. Other ESL models can be found in [9, 10]. On the other hand, in Layer Wise

*Address all correspondence to this author.

(LW) methods there is a dependency between the number of unknowns and the number of layers. They have been adopted in many works since they overcome some of the limitations of the ESL approach by accounting the properties of each layer separately. Some studies on LW models are included in [11–13].

The geometric approximation of the problem is directly related to the accuracy of finite element models. The most common approaches are briefly discussed in the following. According to Szabó and Babŭska [14], the finite element space is characterized by three factors: the finite element mesh, the polynomial order of the elements and the mapping functions. A proper combination of these parameters is needed to minimize the approximation error of any structural problem. Conventional finite element methods follow an *h*-refinement scheme to increase the accuracy by refining the finite element mesh. Isoparametric elements, which employ the same shape functions to interpolate both the solutions and the geometry, are used to approximate curves and surface boundaries. On the other hand, the *p*-version of the finite element method make use of a fixed mesh and, as a consequence, the quality of the approximation depends on the polynomial degree of the elements. Due to the coarse discretizations normally used in *p*-models, a proper representation of the geometric domain is required to reduce the approximation error. In this context, Gordon and Hall [15] presented a method in which parametric polynomials are employed to represent the shape of curved boundaries, denoted as the blending function method. These polynomials are opportunely introduced into the mapping functions of the elements, increasing in this manner the quality of the approximation. This method has been successfully applied for the modelling of curved domains of *p*-version finite elements in several works, such as [16, 17].

The main focus of the present research is to use the blending function method and the concept of non-isoparametric mapping for the description of the cross-section of beam models, while the longitudinal axis is discretized by conventional Lagrange-type beam elements. This procedure allows one to represent the exact shape of the beam section and, consequently, to reduce the error of the geometric approximation. The component-wise (CW) approach is recalled in this work and applied to generate global-local models in which the different-level components of laminates (layers, fibers and matrices) can be formulated simultaneously. CW models have been employed successfully for the analysis of multi-component structures in many works, for example [18–21]. Hierarchical Legendre Expansions (HLE), introduced in Carrera et al. [22], are used in this work to spread the unknowns over the cross-section domain with hierarchical higher-order polynomials, for which the mapping techniques can be better exploited.

The Carrera Unified Formulation (CUF), developed during the last years by Carrera and its colleagues [23, 24], has been extensively employed to obtain refined models for the analysis of composite structures. The effectiveness of CUF beam models

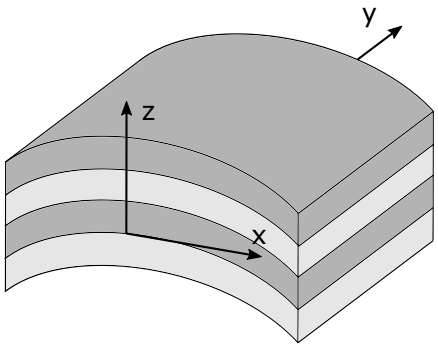


**FIGURE 1**. COORDINATE FRAME OF A LAMINATED BEAM.

accounting both ESL and LW approaches was presented in [25] and a series of refined theories based on Taylor's polynomials, trigonometric series, hyperbolic, exponential, and zig-zag functions were introduced in [26], showing the generality of the formulation. Many other applications of CUF on composites can be found in the literature, including multi-line models [27], analysis of composite rotors [28] and thin-walled structures [29]. A brief introduction to the different theories based on CUF is included in the following sections, with a focus on the mapping technique employed at the cross-sectional level and its application on composite materials. Some numerical solutions are then provided to validate the method, and the main conclusions are outlined.

## PRELIMINARIES

Let us consider a Cartesian reference system like the one shown in Fig 1. The longitudinal axis of the beam coincides with the *y*-coordinate, whereas the cross-section, $\Omega$, is placed on the *xz*-plane. The cross-section of the beam contains an arbitrary number of layers with curved boundaries. In this framework, the associated displacement field reads

$$\mathbf{u}(x,y,z) = \left\{ \begin{array}{c} u_x(x,y,z) \\ u_y(x,y,z) \\ u_z(x,y,z) \end{array} \right\} \tag{1}$$

The strain and stress components can be grouped in six-term vectors as

$$\begin{aligned} \boldsymbol{\varepsilon}^T &= \left\{ \varepsilon_{yy} \ \varepsilon_{xx} \ \varepsilon_{zz} \ \varepsilon_{xz} \ \varepsilon_{yz} \ \varepsilon_{xy} \right\} \\ \boldsymbol{\sigma}^T &= \left\{ \sigma_{yy} \ \sigma_{xx} \ \sigma_{zz} \ \sigma_{xz} \ \sigma_{yz} \ \sigma_{xy} \right\} \end{aligned} \tag{2}$$

and the geometrical relations between strains and displacements, using this vectorial notation, are

$$\boldsymbol{\varepsilon} = \mathbf{D}\,\mathbf{u} \tag{3}$$

where $\mathbf{D}$ is a $6 \times 3$ matrix that contains the differential operators $\frac{\partial}{\partial x}$, $\frac{\partial}{\partial y}$ and $\frac{\partial}{\partial z}$. Finally, the stress components can be obtained through the constitutive laws, that make use of the stiffness matrix to relate strains and stresses as follows

$$\boldsymbol{\sigma} = \tilde{\mathbf{C}}\boldsymbol{\varepsilon} \tag{4}$$

The coefficients $\tilde{C}_{ij}$ of the stiffness matrix are not included here for the sake of brevity. They depend on the mechanical properties of the material and the orientation of the fibers of each layer in relation with the global coordinates defined in Fig. 1.

## REFINED BEAM MODELS BASED ON CUF

A usual method used by researchers to overcome the limitations of conventional beam theories is to enrich the kinematic field with additional terms, enabling to capture higher-order effects within the cross-section. In the framework of CUF, the displacement field is described in a unified manner by expanding the unknown variables over the section domain with generic functions, as

$$\mathbf{u}(x,y,z) = F_\tau(x,z)\mathbf{u}_\tau(y) \quad \tau = 1,2,...,M \tag{5}$$

where $\tau$ denotes summation. $u_\tau(y)$ is the vector of general displacements and $M$ the number of terms of the expansion. $F_\tau$ represents the set of expansion functions and determines the theory of structure to be used in the beam formulation. Many theories of structure have been developed via the Unified Formulation during the last years, including Taylor-based Expansions (TE) and Lagrange-based Expansions (LE). Hierarchical Legendre Expansions have been recently implemented in the framework of CUF and their performance in the analysis of laminates has been assessed in Pagani et al. [30]. To be concise, only a brief introduction of HLE is addressed bellow these lines.

For HLE theories, the $F_\tau$ expansions are defined from Legendre-class polynomials. HLE models make use of a hierarchical set of these polynomials to generate quadrilateral expansion domains that are employed to discretize the physical surface of the cross-section. The main feature of this kind of models is that the polynomial order of the theory, $p$, is introduced as an input parameter, allowing one to select the accuracy of the solutions. Vertex, edge and internal functions conform the expansion space, as shown in Fig. 2.

**Vertex expansions** The nodal or vertex modes are defined as bi-linear functions that take the value 1 in one vertex and 0 in the rest, as

$$F_\tau = \frac{1}{4}(1+r_i r)(1+s_i s) \quad \tau = 1,2,3,4 \tag{6}$$

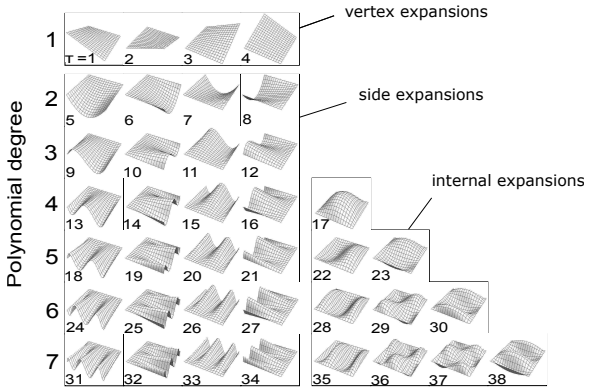


**FIGURE 2**. HIERARCHICAL SET OF LEGENDRE-TYPE FUNCTIONS USED AS $F_\tau$ IN HLE MODELS.

where $r$ and $s$ vary over the domain between $-1$ and $+1$, and $r_\tau$ and $s_\tau$ correspond to the vertex location in the natural system of coordinates.

**Side expansions** The side modes are accounted for $p \geq 2$ and they are null at all edges but one. Their expressions are:

$$F_\tau(r,s) = \frac{1}{2}(1-s)\phi_p(r) \quad \tau = 5,9,13,18,... \tag{7}$$

$$F_\tau(r,s) = \frac{1}{2}(1+r)\phi_p(s) \quad \tau = 6,10,14,19,... \tag{8}$$

$$F_\tau(r,s) = \frac{1}{2}(1+s)\phi_p(r) \quad \tau = 7,11,15,20,... \tag{9}$$

$$F_\tau(r,s) = \frac{1}{2}(1-r)\phi_p(s) \quad \tau = 8,14,16,21,... \tag{10}$$

where $\phi_p$ correspond to the one-dimensional internal Legendre-type modes. They are not included here, but the lector can find them in [14].

**Internal expansions** They exist for $p \geq 4$ and vanish at all the edges of the quadrilateral domain. For a given expansion order, there are $(p-2)(p-3)/2$ internal polynomials in total. For instance, the set of sixth-order polynomials contains 3 internal expansions (see Fig. 2), defined as the product of 1D internal modes,

$$F_{28}(r,s) = \phi_4(r)\phi_2(s) \tag{11}$$

$$F_{29}(r,s) = \phi_3(r)\phi_3(s) \tag{12}$$

$$F_{30}(r,s) = \phi_2(r)\phi_4(s) \tag{13}$$

The hierarchic features of HLE models are due to the fact that for a particular order $p*$, introduced as an input, the set of expansion functions includes all the polynomials of order $p \leq p*$,

and so does the displacement field. This characteristic in conjunction with the CW method allow us to obtain highly accurate models for any geometry of the cross-section.

The beam axis is discretized by means of the finite element method. In one-dimensional elements, the generalized displacements can be written as a function of the unknown nodal vector, $\mathbf{q}_{\tau i}$, and the 1D interpolation functions, $N_i$, as follows

$$\mathbf{u}_\tau(y) = N_i(y)\mathbf{q}_{\tau i}, \qquad i = 1,2,...,n_n \tag{14}$$

where $i$ denotes summation and $n_n$ is the number of nodes per beam element. Many beam models can be formulated depending on the choice of the shape functions $N_i$. In the present work, cubic Lagrange-type polynomials have been employed to interpolate the displacement unknowns on the element nodes.

The Principle of Virtual Displacements (PVD) is recalled to obtain the governing equations. The PVD states that the virtual variation of internal work must be equal to the virtual variation of the external work for the structure to be in equilibrium. The internal work is defined as

$$\delta L_{int} = \int_l \int_\Omega \delta\boldsymbol{\varepsilon}^T \boldsymbol{\sigma}\, d\Omega\, dy \tag{15}$$

Now, if one consider de geometrical relations (Eq. (3)), the constitutive law (Eq. (4)), and the expressions related to the CUF kinematic field (Eq. (5)) and the FEM discretization (Eq. (14)), the formal definition of the internal work can be rewritten as

$$\delta L_{\text{int}} = \delta \mathbf{q}_{\tau i}^T \mathbf{K}^{\tau s i j} \mathbf{q}_{sj} \tag{16}$$

where $\boldsymbol{K}^{\tau s i j}$ is the fundamental nucleus of the stiffness matrix. These matrices are $3 \times 3$ arrays that contain the essential information of the model. For the sake of brevity, only one of its components is reported here, but a complete descrption can be found in [30], for instance.

$$\begin{aligned} K_{11}^{\tau s i j} = {} & \widetilde{C}_{22} \int_l N_i N_j \,\mathrm{d}y \int_\Omega F_{\tau,x} F_{s,x}\, d\Omega + \widetilde{C}_{44} \int_l N_i N_j \,\mathrm{d}y \int_\Omega F_{\tau,z} F_{s,z}\, d\Omega + \\ & \widetilde{C}_{26} \int_l N_i N_{j,y} \,\mathrm{d}y \int_\Omega F_{\tau,x} F_s\, d\Omega + \widetilde{C}_{26} \int_l N_{i,y} N_j \,\mathrm{d}y \int_\Omega F_\tau F_{s,x}\, d\Omega + \\ & \widetilde{C}_{66} \int_l N_{i,y} N_{j,y} \,\mathrm{d}y \int_\Omega F_\tau F_s\, d\Omega \end{aligned} \tag{17}$$

It can be noticed that the fundamental nuclei depend on the material coefficients, $\tilde{C}_{ij}$, the integrals of the shape functions along the axis, $l$, and the integrals of the expansion functions over the cross-section domain, $\Omega$. The main advantage of CUF is that any-order and class theories can be formulated with only nine FORTRAN statements.

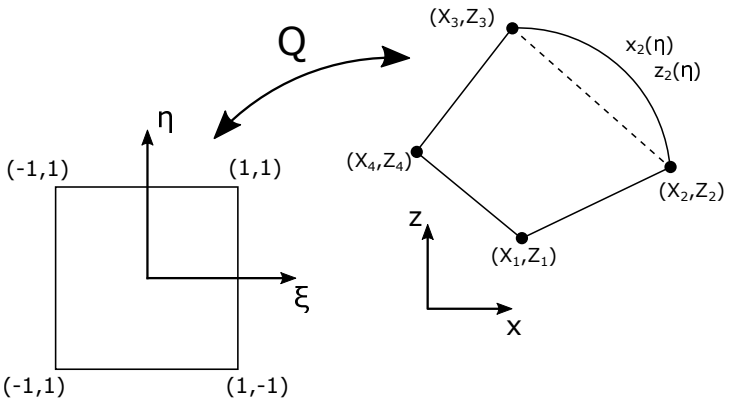


**FIGURE 3**. MAPPING OF A CROSS-SECTION DOMAIN BY THE BLENDING FUNCTION METHOD.

### Cross-Section Mapping

As it has been introduced before, the higher-order polynomials usually utilized in HLE models enable the use of coarse discretizations of the cross-section domain without any loss of accuracy. The blending function method is employed in this paper to represent the exact shape of curved boundaries in large expansion domains. This method will allow us to model, for instance, the fiber section with only one domain, or to capture any curved geometry without the need of refining the discretization. The concept is illustrated in Fig. 3, in which a quadrilateral domain with a curved side is considered. The mapping functions in the cross-section plane for this case can be written as:

$$\begin{aligned} Q_x(\xi,\eta) &= \sum_{i=1}^{4} F_i(\xi,\eta) X_i + (x_2(\eta) - (\frac{1-\eta}{2} X_2 + \frac{1+\eta}{2} X_3)) \frac{1+\xi}{2} \\ Q_z(\xi,\eta) &= \sum_{i=1}^{4} F_i(\xi,\eta) Z_i + (z_2(\eta) - (\frac{1-\eta}{2} Z_2 + \frac{1+\eta}{2} Z_3)) \frac{1+\xi}{2} \end{aligned} \tag{18}$$

The first term correspond to the linear isoparametric mapping functions, whereas the second basically converts the straight line that links vertices 2 and 3 into the curved shape determined by $x_2(\eta)$ and $z_2(\eta)$. The blending function method in conjunction with HLE models allow us to model the exact shape of any section geometry with a reduced number of expansions, which leads to a reduced computational cost.

## NUMERICAL RESULTS

Some static analysis are addressed in this section. First, a slender sandwich panel with a curved section has been considered. After this assessment, a micro-scale study of a fiber-matrix cell and a cross-ply laminated beam are included. The advantages of the present formulation in the analysis of laminated structures are opportunely commented. Ten Lagrange-type beam elements with four-nodes are employed for the longitudinal mesh

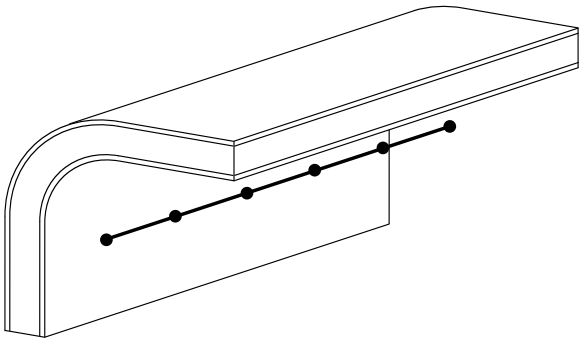

**FIGURE 4**. REPRESENTATION OF THE CURVED SANDWICH BEAM MODEL.

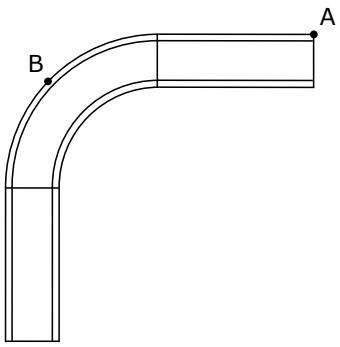


**FIGURE 5**. CROSS-SECTION DOMAIN DISTRIBUTION OF THE CURVED SANDWICH BEAM.

along the $y$-axis in all the examples. This mesh configuration has been selected to ensure convergent results. The HLE beam models are compared with solid and shell solutions obtained from the commercial software MSC Nastran as well as other beam theories.

### Curved Sandwich

An L-angle curved sandwich is considered for the first assessment to validate the present formulation on multi-component configurations. Figure 4 shows a representation of the beam model used in this study. The panel's length is 1 m and the global geometric features of the cross-section are 40 mm high, 40 mm wide and 7 mm thick. A quarter-circumference segment links the flange and the web, being the radius of the outer boundary as high as 20 mm. The sandwich is composed of two Aluminum faces of 1 mm each and a foam core of 5 mm of thickness. Both components are modeled as isotropic materials, being their properties: for the Aluminum, Young's modulus, $E$, equals to 75 GPa and Posisson ratio, $\nu$, 0.33; for the foam, $E$ equals to 0.1063 GPa and $\nu$ is 0.32. A clamped-free configuration is selected, and a pressure of 10 kN/m$^2$ is applied on the top surface of the straight flange, pushing the structure downwards. The cross-section domain distribution is reported in Fig. 5. Each component is modeled with three local expansions, which are curved in the middle segment of the section. Polynomial orders from $2^{nd}$ to $8^{th}$ (HL2 - HL8) have been considered for the expansion functions over the cross-section. Cubic mapping functions are employed to accurately represent the geometry of the curved domains.

The numerical results of displacements and stresses are addressed in Table 1. Shell and solid NASTRAN elements are used to validate the solutions. The vertical displacements, $u_z$, are measured at the upper corner of the section (Point A in Fig. 5) at the tip, whereas the normal and shear stress solutions, $\sigma_{yy}$ and $\sigma_{yz}$ respectively, are evaluated at the midpoint of the outer surface of the curved segment (point B) at the middle section. The mixed interpolation of tensorial components (MITC) method has been employed to mitigate the shear locking phenomenon and to obtain the correct distribution of shear stresses, see Carrera et al. [31]. Finally, the right-hand column of the table shows the degrees of freedom of each model. Fig. 6 displays the normal and shear stress distribution along the thickness of the sandwich at Point B. Finally, Fig. 7 and 8 show a 2D plot of the normal and shear stresses, respectively, at the middle section, showing the capabilities of refined CUF models of reproducing 3D-like solutions through one-dimensional models. Out of these results we can state that:

1. HLE solutions are in good agreement with the results obtained from solid elements in NASTRAN, and clearly overcome those of the shell elements. Convergence in the displacements is reached from the $3^{rd}$ expansion order (HL3 model). Both normal and shear stress distribution are correctly captured with an important reduction in the computational cost.
2. The mapping technique enables HLE models to reproduce the exact shape of the section with a few local expansions. The accuracy of the results is not compromised since the polynomial order of the expansions can be set to a desired level of accuracy.

### Fiber-Matrix Cell

A mechanical study of the fiber-matrix cell is conducted at a micro-scale level in the following example. The fiber has been assumed as cylindrical, and the matrix is perfectly bounded around it, conforming a rectangular block. The complete composite is then modeled as a square beam with the following geometric sizes: side of the square section, $b$, equals to 0.1 mm, diameter of the fiber, $d$, equals to 0.08 mm and length, $L$, is as high as 4 mm. Both the matrix and the fiber have been considered isotropic. The Young's modulus, $E$, of the fiber is equal to 202.038 GPa and its Poisson ratio, $\nu$, is 0.2128. For the matrix material, $E = 3.252$ GPa and $\nu = 0.355$. The structure is

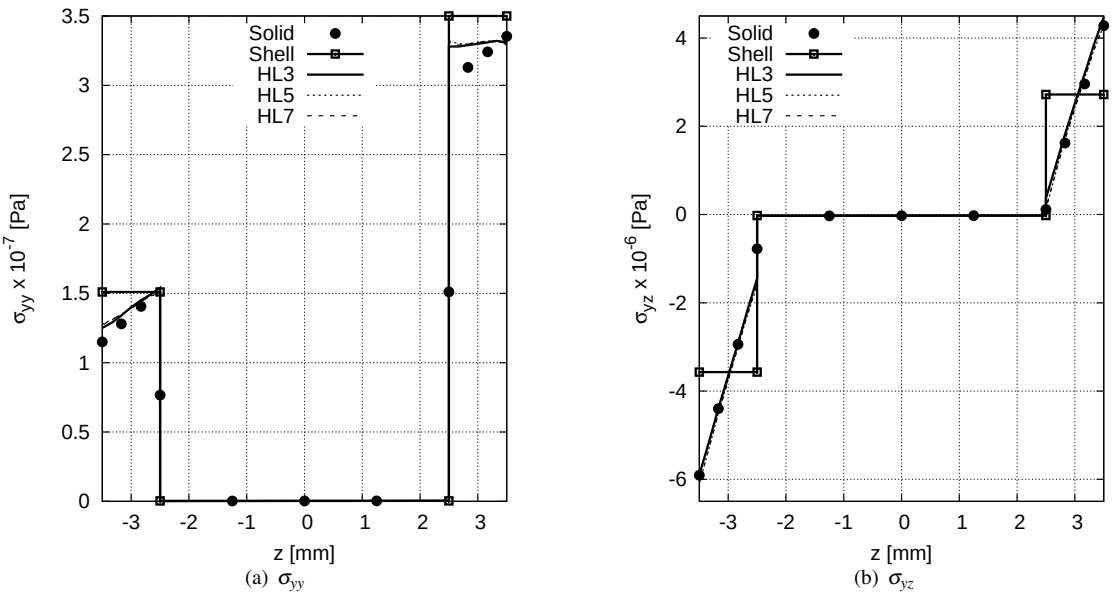


**FIGURE 6**. NORMAL AND SHEAR STRESSES ALONG THE THICKNESS AT POINT B, Y=L/2.

**TABLE 1**. RESULTS OF DISPLACEMENTS AND STRESSES OF THE CURVED SANDWICH BEAM.

| model | $u_z \times 10^2$ m | $\sigma_{yy} \times 10^{-7}$ Pa | $\sigma_{yz} \times 10^{-6}$ Pa | DOFs |
|---|---|---|---|---|
| | Point A | point B | Point B | |
| MSC Nastran solutions | | | | |
| Solid | -3.715 | 3.353 | 4.324 | 166617 |
| Shell | -3.900 | 3.496 | 2.721 | 71000 |
| HLE model solutions | | | | |
| HL2 | -3.032 | 3.421 | -6.551 | 3720 |
| HL3 | -3.711 | 3.307 | 4.484 | 5952 |
| HL4 | -3.712 | 3.293 | 4.466 | 9021 |
| HL5 | -3.712 | 3.288 | 4.276 | 12927 |
| HL6 | -3.712 | 3.290 | 4.256 | 17670 |
| HL7 | -3.712 | 3.298 | 4.308 | 23250 |
| HL8 | -3.712 | 3.297 | 4.321 | 29667 |

clamped at one edge and a vertical load, $F_z = -0.1$ N, is applied at the other one, at the center of the section $[0, L, 0]$. All the evaluating points are included considering a reference system equivalent to the one of Fig. 1 and placed at the center of the cell. Fig. 9 shows the differences in the cross-section domain discretization for conventional CUF LE models and the novel HLE model. The blending function method enables to model the fiber section

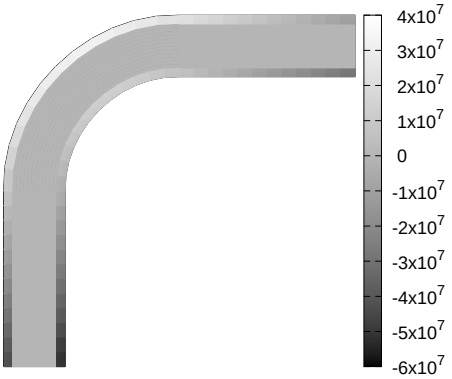


**FIGURE 7**. NORMAL STRESSES [PA] AT THE MIDDLE SECTION OF THE CURVED SANDWICH BEAM, HL5 MODEL.

with only one expansion domain, summing five domains for the entire cell, whereas isoparametric LE models require at least 20 domains (12 nine-node L9 + 8 six-node L6) to approximate the geometry.

Table 2 presents the displacements and stress solutions at various points of the structure, together with the DOFs of each model. The results are validated with solid element solutions of NASTRAN. Classic beam theories of Euler and Timoshenko, TE and LE models have also been included for comparison purposes. The TE models here addressed have been generated by us-

**TABLE 2**. DISPLACEMENTS AND STRESS RESULTS OF THE FIBER-MATRIX CELL IN VARIOUS POINTS.

| model | $u_z$ | $\sigma_{yy}$ | $\sigma_{yy}$ | $\sigma_{yz}$ | DOFs |
|---|---|---|---|---|---|
| | $[0,L,0]$ | $[0,L/2,d/2]$ | $[0,L/2,0.03]$ | $[-d/2,L/2,d/2]$ | |
| MSC Nastran model [18] | | | | | |
| SOLID | -7.818 | 9.492 | 7.094 | -2.383 | 268215 |
| Classical and refined models based on TE [18] | | | | | |
| EBBT | -7.811 | 9.469 | 7.102 | -1.962 | 363 |
| TBT | -7.835 | 9.469 | 7.102 | -1.962 | 605 |
| N=1 | -7.835 | 9.469 | 7.102 | -1.962 | 1089 |
| N=2 | -7.774 | 9.358 | 7.019 | -2.311 | 2178 |
| N=3 | -7.777 | 9.358 | 7.019 | -2.464 | 3630 |
| N=4 | -7.794 | 9.327 | 7.090 | -2.454 | 5445 |
| N=5 | -7.795 | 9.327 | 7.090 | -2.375 | 7623 |
| N=6 | -7.800 | 9.315 | 7.105 | -2.373 | 10164 |
| N=7 | -7.800 | 9.315 | 7.105 | -2.304 | 13068 |
| N=8 | -7.804 | 9.346 | 7.117 | -2.301 | 16335 |
| LE models [18] | | | | | |
| 12L9+8L6 | -7.933 | 9.450 | 7.046 | -2.500 | 7533 |
| HLE models | | | | | |
| HL1 | -0,459 | 9.966 | 7.287 | 1.340 | 744 |
| HL2 | -2.616 | 2.532 | 1.861 | -7.315 | 1860 |
| HL3 | -7.763 | 9.358 | 7.092 | -3.212 | 2976 |
| HL4 | -7.771 | 9.400 | 7.071 | -2.912 | 4557 |
| HL5 | -7.773 | 9.383 | 7.070 | -2.746 | 6603 |
| HL6 | -7.774 | 9.412 | 7.080 | -2.296 | 9114 |
| HL7 | -7.775 | 9.365 | 7.073 | -3.219 | 12090 |
| HL8 | -7.775 | 9.361 | 7.071 | -3.556 | 15531 |

ing McLaurin polynomial expansions of up to $8^{th}$ order, whereas LE models employ Lagrange-class bi-quadratic expansions. It is possible to state that all beam models present a good performance, being able to obtain very close values to the solid model with a great reduction in number of DOFs. To complete the assessment, the normal and shear stress distributions at the middle section obtained with HLE mapped models are shown in Fig. 10.

### Cross-Ply

The fiber-matrix cell configuration above presented is now used to conform a symmetric $[0^\circ, 90^\circ, 0^\circ]$ cross-ply beam model. A set of these cells is grouped to model the $0^\circ$ layers, see Fig. 11, while the $90^\circ$ ply is modelled with an orthotropic material of equivalent properties. In this case, the fiber is considered orthotropic, with $E_L = 202.038$ GPa; $E_T = E_z = 12.134$ GPa; $G_{LT} = 8.358$ GPa; $G_{Lz} = 8.358$ GPa; $G_{Tz} = 47.756$ GPa; $\nu_{LT} = 0.2128$; $\nu_{Lz} = 0.2128$ and $\nu_{Tz} = 0.2704$. The matrix is modeled as isotropic instead, with $E = 3.252$ GPa and $\nu = 0.355$.

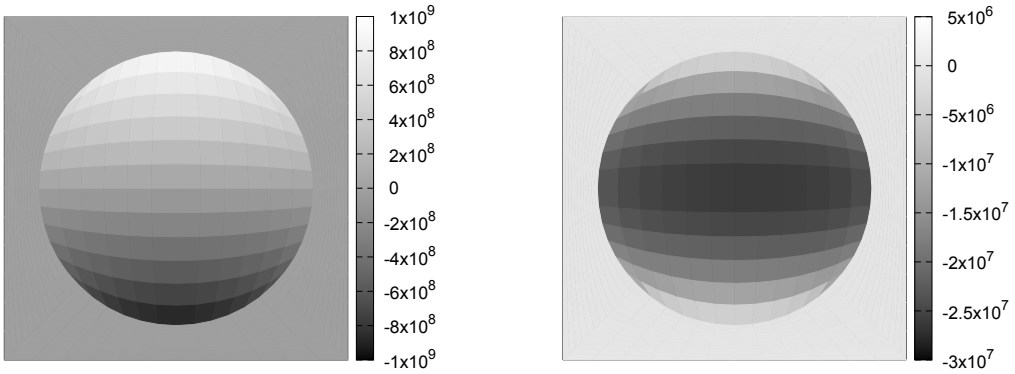


(a) $\sigma_{yy}$ (b) $\sigma_{yz}$

**FIGURE 10**. NORMAL AND SHEAR STRESS DISTRIBUTIONS [PA] AT THE MIDDLE SECTION OF THE FIBER-MATRIX CELL, HL6 MODEL.

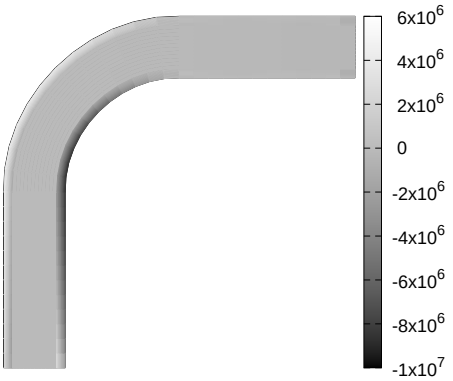


**FIGURE 8**. SHEAR STRESSES [PA] AT THE MIDDLE SECTION OF THE CURVED SANDWICH BEAM, HL5 MODEL.

The equivalent properties of the layer are: $E_L = 103.173$ GPa; $E_T = E_z = 5.145$ GPa; $G_{LT} = 2.107$ GPa; $G_{Lz} = 2.107$ GPa; $G_{Tz} = 2.353$ GPa; $\nu_{LT} = 0.2835$; $\nu_{Lz} = 0.2835$ and $\nu_{Tz} = 0.3124$. The beam is 40 mm long, 0.6 mm high and 0.8 mm wide, being the characteristics of each cell: $b$ equals to 0.2 mm and $d$ equals to 0.16 mm. The CW approach allow us to consider layers, fibers and matrices within the same model without any loss of generality.

A convergence study of the results in terms of displacements and stresses is addressed in Table 3. The solution points are also included in the table according to a reference system placed at the middle of the left edge of the clamped section. All the results converge for the $3^{rd}$ expansion order (HL3 model). Fig. 12 shows both the normal and shear stress distributions at the middle section. These results demonstrate the potential of the present beam model in capturing complex states of stress in fiber-reinforced laminates at a global-local level. The main remarks extracted from this study are presented in the following conclusions.

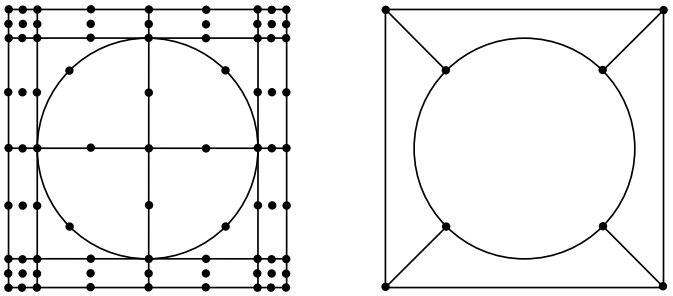

(a) LE (b) HLE

**FIGURE 9**. CROSS-SECTION DOMAIN DISTRIBUTIONS OF THE FIBER-MATRIX CELL FOR LE AND HLE MODELS.

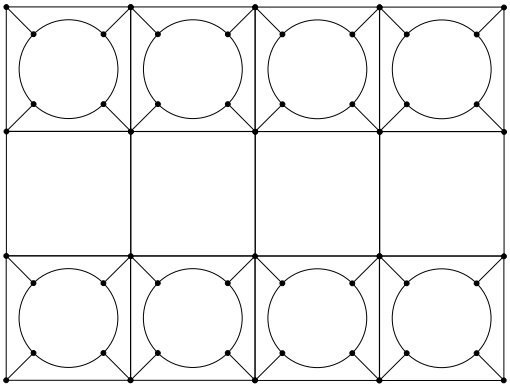

**FIGURE 11**. CROSS-SECTION DOMAIN DISTRIBUTION OF THE CROSS-PLY.

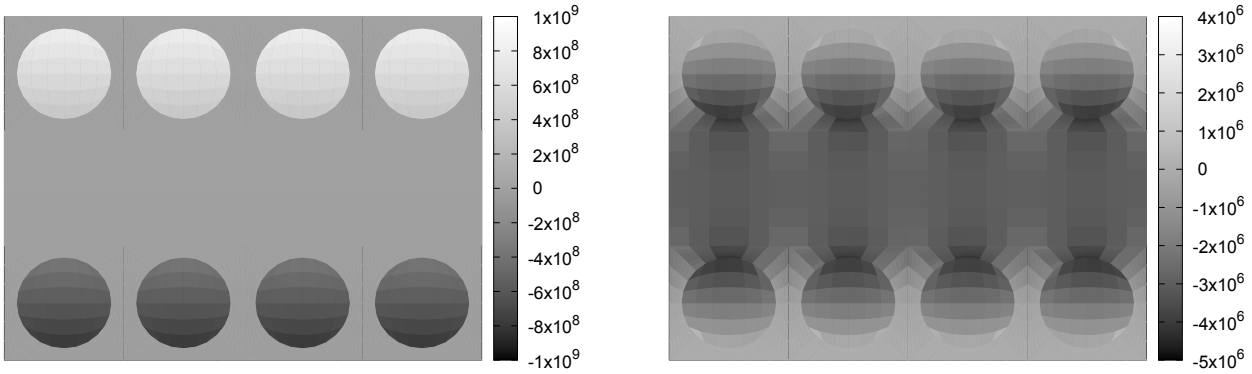


(a) $\sigma_{yy}$ (b) $\sigma_{yz}$

**FIGURE 12**. NORMAL AND SHEAR STRESS DISTRIBUTIONS [PA] AT THE MIDDLE SECTION OF THE CROSS-PLY BEAM, HL5 MODEL.

**TABLE 3**. RESULTS OF DISPLACEMENTS AND STRESSES OF THE CROSS-PLY BEAM IN VARIOUS POINTS.

| model | $u_z$ mm | $\sigma_{yy} \times 10^2$ Mpa | $\sigma_{yz}$ Mpa | DOFs |
|---|---|---|---|---|
| | [0.4, L, 0] | [0.5, L/2, -0.2] | [0.5, L/2, -0.2] | |
| HL1 | -0.053 | -0.017 | -29.309 | 4836 |
| HL2 | -0.348 | -0.838 | -43.008 | 13671 |
| HL3 | -1.547 | -5.849 | -2.389 | 22506 |
| HL4 | -1.548 | -5.848 | -2.445 | 35433 |
| HL5 | -1.548 | -5.848 | -2.432 | 52452 |
| HL6 | -1.548 | -5.848 | -2.422 | 73563 |

## CONCLUSIONS

A novel hierarchical one-dimensional method based on the Carrera Unified Formulation has been presented in this work. HLE models have demonstrated many advantages in the analysis of composite structures at both global and local scales. The construction of the physical model is substantially simplified due to two facts: first, the discretization of the cross-section domain is fixed and can be optimized, and second, the level of accuracy depends in a great manner on the polynomial order of the model. As a consequence, there is no need of performing iterative refinements to increase the precision of the solution, which is one of the most time-consuming works in conventional finite element methods. These capabilities are greatly enforced by the use of mapping techniques that allow to represent the exact shape of the section geometry and to better optimize the distribution of local expansions. In addition, the CW approach enables to direct the precision of the model to particular zones of interest within the cross-section, augmenting considerably the efficiency of the computation.

## ACKNOWLEDGMENT

This research has been carried out within the project FULLCOMP - FULLy analysis, design, manufacturing, and health monitoring of COMPosite structures - funded by the Marie Sklodowska-Curie actions grant agreement no. 642121. The H2020 European Training Networks are gratefully acknowledged.

## REFERENCES

[1] Tsai, S. W., 1988. *Composites Design*, 4th ed. Dayton, Think Composites.

[2] Euler, L., 1744. *De curvis elasticis*. Lausanne and Geneva: Bousquet.

[3] Timoshenko, S. P., 1922. "On the transverse vibrations of bars of uniform cross section". *Philosophical Magazine,* ***43***, pp. 125–131.

[4] Kapania, R., and Raciti, S., 1989. "Recent advances in analysis of laminated beams and plates, part I: Shear effects and buckling". *AIAA Journal,* ***27***(7), pp. 923–935.

[5] Kapania, R., and Raciti, S., 1989. "Recent advances in analysis of laminated beams and plates, part II: Vibrations and wave propagation". *AIAA Journal,* ***27***(7), pp. 935–946.

[6] Reddy, J. N., 1986. "A simple higher-order theory for laminated composites". *Journal of Applied Mechanics,* ***51***, pp. 745–752.

[7] Khdeir, A., and Reddy, J., 1994. "Free vibration of cross-ply laminated beams with arbitrary boundary conditions". *International Journal of Engineering Science,* ***32***(12), pp. 1971 – 1980.

[8] Khdeir, A., and Reddy, J., 1997. "Buckling of cross-ply laminate beams with arbitrary boundary conditions". *Composite Structures,* ***37***, pp. 1–3.

[9] Matsunaga, H., 2002. "Interlaminar stress analysis of laminated composite beams according to global higher-

order deformation theories". *Composite Strucutures,* ***55***, pp. 105–114.

[10] Vidal, P., Gallimard, L., and Polit, O., 2012. "Composite beam finite element based on the proper generalized decomposition". *Computers & Structures,* ***102103***, pp. 76 – 86.

[11] Shimpi, R. P., and Ghugal, Y. M., 2001. "A new layerwise trigonometric shear deformation theory for two-layered cross-ply beams". *Composites Science and Technology,* ***61***(9), pp. 1271 – 1283.

[12] Surana, K., and Nguyen, S., 1990. "Two-dimensional curved beam element with higher-order hierarchical transverse approximation for laminated composites". *Computers and Structures,* ***36***, pp. 499–511.

[13] Ferreira, A. J. M., 2005. "Analysis of composite plates using a layerwise theory and multiquadrics discretization". *Mechanics of Advanced Materials and Structures,* ***12***(2), pp. 99–112.

[14] Szabó, B., and Babuka, I., 1991. *Finite Element Analysis*. John Wiley and Sons, Ltd.

[15] Gordon, W., and Hall, C. "Transfinite element methods: Blending-function interpolation over arbitrary curved element domains". *Numerische Mathematik,* ***21***(2), pp. 109–129.

[16] Düster, A., Bröker, H., and Rank, E., 2001. "The p-version of the finite element method for three-dimensional curved thin walled structures". *International Journal for Numerical Methods in Engineering,* ***52***(7), pp. 673–703.

[17] Kirlyfalvi, G., and Szabó, B. A., 1997. "Quasi-regional mapping for the p-version of the finite element method". *Finite Elements in Analysis and Design,* ***27***(1), pp. 85 – 97. Robert J. Melosh Medal Competition.

[18] Carrera, E., Maiarù, M., and Petrolo, M., 2012. "Component-wise analysis of laminated anisotropic composites". *International Journal of Solids and Structures,* ***49***, pp. 1839–1851.

[19] Carrera, E., Pagani, A., and Petrolo, M., 2013. "Component-wise method applied to vibration of wing structures". *Journal of Applied Mechanics,* ***80***(4), p. 041012.

[20] Carrera, E., Pagani, A., and Petrolo, M., 2013. "Classical, refined and component-wise theories for static analysis of reinforced-shell wing structures". *AIAA Journal,* ***51***(5), pp. 1255–1268.

[21] Carrera, E., Pagani, A., and Petrolo, M., 2015. "Refined 1D finite elements for the analysis of secondary, primary, and complete civil engineering structures". *Journal of Structural Engineering,* ***141***, pp. 04014123/1–14.

[22] Carrera, E., de Miguel, A., and Pagani, A., 2016. "Hierarchical theories of structures based on Legendre polynomial expansions with finite element applications". Submitted.

[23] Carrera, E., 2002. "Theories and finite elements for multi-layered, anisotropic, composite plates and shells". *Archives of Computational Methods in Engineering,* ***9***(2), pp. 87–140.

[24] Carrera, E., and Petrolo, M., 2012. "Refined beam elements with only displacement variables and plate/shell capabilities". *Meccanica,* ***47***(3), pp. 537–556.

[25] Carrera, E., and Petrolo, M., 2012. "Refined one-dimensional formulations for laminated structure analysis". *AIAA Journal,* ***50***(1), pp. 176–189.

[26] Carrera, E., and Filippi, M.and Zappino, E., 2013. "Laminated beam analysis by polynomial, trigonometric, exponential and zig-zag theories". *European Journal of Mechanics A/Solids*. Published.

[27] Carrera, E., and Pagani, A., 2014. "Multi-line enhanced beam model for the analysis of laminated composite structures". *Composites: Part B,* ***57***, pp. 112–119.

[28] Carrera, E., Filippi, M., and Zappino, E., 2013. "Free vibration analysis of rotating composite blades via carrera unified formulation". *Composite Structures,* ***106***, pp. 317–325.

[29] Carrera, E., Filippi, M., Mahato, P., and Pagani, A., 2016. "Accurate static response of single- and multi-cell laminated box beams". *Composite Structures,* ***136***, pp. 372–383.

[30] Pagani, A., de Miguel, A., Petrolo, M., and Carrera, E., 2016. "Analysis of laminated beams via Unified Formulation and Legendre polynomial expansions". *Composite Structures*. In press.

[31] Carrera, E., de Miguel, A., and Pagani, A., 2016. "Higher-order MITC beam elements based on the Unified Formulation". In submission.